Journal of Power Sources 209 (2012) 236–242

Contents lists available at SciVerse ScienceDirect

Journal of Power Sources

journal homepage: www.elsevier.com/locate/jpowsour

Palladium nanocrystals supported on helical carbon nanofibers for highly efficient electro-oxidation of formic acid, methanol and ethanol in alkaline electrolytes

Guangzhi Hu[a,1], Florian Nitze[a,1], Hamid Reza Barzegar[a], Tiva Sharifi[a], Ania Mikołajczuk[b], Cheuk-Wai Tai[c], Andrzej Borodzinski[b], Thomas Wågberg[a,*]

[a] Department of Physics, Umeå University, S-901 87 Umeå, Sweden
[b] Institute of Physical Chemistry, Polish Academy of Sciences, 01-224 Warszawa, Poland
[c] Department of Materials and Environmental Chemistry, Arrhenius Laboratory, Stockholm University, S-106 91 Stockholm, Sweden

ARTICLE INFO

Article history:
Received 18 October 2011
Received in revised form 20 February 2012
Accepted 21 February 2012
Available online 3 March 2012

Keywords:
Helical carbon fibers
Electrocatalysts
Palladium
Nanoparticles
Electron microscopy
Fuel cells

ABSTRACT

We present the synthesis of palladium nanocrystals self-assembled on helical carbon nanofibers functionalized with benzyl mercaptan (Pd-S-HCNFs) and their electrocatalytic activity toward the oxidation of formic acid, methanol and ethanol. Helical carbon nanofibers (HCNFs) were first functionalized with benzyl mercaptan based on the π–π interactions between phenyl rings and the graphitic surface of HCNFs. Palladium nano crystals (PdNC) were fixed on the surface of functionalized HCNF by Pd—S bonds in a simple self-assembly method. The as-prepared materials were characterized by high resolution transmission electron microscopy (HR-TEM), X-ray photoelectron spectroscopy (XPS) and X-ray diffraction (XRD), energy dispersive X-ray spectroscopy (EDX), cyclic voltammetry (CV), and fuel cell tests. CV characterization of the as-prepared materials shows a very high electrocatalytic activity for oxidation of formic acid, ethanol and methanol in strong alkaline electrolyte. In comparison to commercial catalyst Vulcan XC-72 decorated with Pd nanoparticles, the proposed Pd-S-HCNFs nano composite material shows oxidation currents for formic acid, ethanol and methanol at the Pd-S-HCNF-modified electrode that are higher than that at the Pd/XC-72 modified electrode with a factor of 2.0, 1.5, and 2.3, respectively. In a formic acid fuel cell the Pd-S-HCNF modified electrode yields equal power density as commercial Pd/XC-72 catalyst. Our results show that Pd-decorated helical carbon nanofibers with diameters around 40–60 nm have very high potential as active material in fuel cells, electrocatalysts and sensors.

1. Introduction

Direct alcohol fuel cells (DAFCs) have received a growing interest in recent years due to the declining resources of fossil fuels and human's responsibility to reduce environmental pollution [1]. There are many different types of fuel cells, such as proton exchange membrane- [2,3], phosphoric acid- [4], alkaline- [5], solid oxide- [6], and molten carbonate fuel cells [4–8]. Among these, proton exchange membrane fuel cells (PEMFC) based on formic acid, methanol, or ethanol have aroused particular interests as a result of their high efficiency, low pollutant emission, low operating temperature (normally below 100 °C), and ease of using liquid fuel [9]. However, some obstacles still limit the application of formic acid, methanol and ethanol fuel cells. Most noteworthy are low electrocatalytic activity of the anode catalysts for formic acid, methanol and ethanol oxidation reactions as well as the high cost of noble metal platinum (Pt) catalyst, which is considered as the best catalyst in low-temperature fuel cells but still is particularly sensitive to CO poisoning [10]. For these reasons development of low-cost non-Pt catalysts with high activity in low temperature fuel cells is highly desirable.

Palladium (Pd) exhibits roughly half the price of Pt and is more abundant in the earth's crust. As catalyst it is still highly active for certain reactions and has good resistance to poisoning, making it to a good candidate in direct-fuel cells [11]. Meanwhile, the catalytic efficiency of Pd-based catalysts crucially depends on its size, morphology, and distribution of the Pd particles [2]. Great efforts have been made to improve the electrocatalytic activity and stability of Pd catalysts. It has been shown that smaller Pd nanoparticles show higher electrochemical activity than that of larger diameter Pd catalysts [12] and that the optimum size for Pd on Vulcan is about 5 nm [13]. Due to its large surface energy and small size, however smaller Pd nanoparticles prepared by chemical reduction

* Corresponding author. Tel.: +46 90 786 5993; fax: +46 90 786 6673.
E-mail address: Thomas.wagberg@physics.umu.se (T. Wågberg).
[1] These authors have equally contributed to the manuscript.

0378-7753/$ – see front matter © 2012 Elsevier B.V. All rights reserved.
doi:10.1016/j.jpowsour.2012.02.080

methods accumulate more easily to form large and irregular Pd black which results in a decreased catalytic activity in fuel cells. To reduce migration and agglomeration of nanocatalysts, surfactants have been applied to control both size and distribution of noble metal nanoparticles [14]. However these surfactant molecules usually adsorb onto the nanoparticles surface which degrades their catalytic performance [15]. A simple method that can load high amounts of small Pd nanoparticles without protective reagents and yet give good catalytic activity, good electrical contact to the support and high stability [16], is thus an important task to enhance the catalytic performance of Pd nanocatalysts. Due to its large area, good conductivity and chemical inertness, carbon-based nanomaterials are ideal in low-temperature fuel cells [17]. Various kinds of Pd- or Pt-carbon supported nanocatalysts have been frequently reported in the last ten years. Zhu et al. [18] used Vulcan XC-72 to support Pd nanoparticles and explored their electrocatalytical activity toward formic acid in acid solutions while Sun et al. [19] synthesized sulfonated ordered mesoporous carbon decorated with Pd nanoparticles with even better electrocatalytic activity than that of Pd/XC-72. In other studies various processes have been applied to decorate nanotubes with Pd, Pt or Pd/Pt nanoparticles and applied them for electrochemical oxidation of methanol [20] and formic acid [21–23]. Recently graphene has also been used as Pd support for the formic acid in fuel cell [24].

Helical carbon nanofibers (HCNF) have an even higher effective surface area than carbon nanotubes since they tend to be less prone to bundle. Still they possess good conductivity and mechanical strength [25]. HCNFs have been grown by several different methods, using Ni—Cu alloys [26], nickel nanoparticles [27] or Fe nanoparticles as catalysts together with pyrolysis of different carbon precursors at 450–650 °C [28] while a low temperature synthesis at 260 °C was reported by Yu et al. [29] by decomposition of acetylene with a catalyst derived from cupric nitrate. No studies so far have focused on using carbon nanofibers as support for nanocatalyst particles. Few studies are reported for the decoration of carbon nanocoils [30,31] but these differs quite significantly from the helical carbon nanofibers regarding the stacking of the graphite layers, the pitch of the coiled fibers as well as their sizes. All these are important parameters that influence the decoration process.

In this report we report a facile, one-pot synthesis of Pd nanocrystal-functionalized HCNF (Pd-S-HCNFs) via a self-assembly method. First, high quality helical carbon nanofibers (more than 90% purity) were synthesized according to our recently presented study [32]. Then HCNFs were functionalized with benzyl mercaptan based on the π–π interaction between benzyl groups and the graphitic surface of HCNF. Pd ions were reduced by hydrazine and strongly fixed by thiol groups on the HCNF surface (Scheme 1). The as-prepared materials were characterized by high resolution transmission electron microscopy (HRTEM), energy dispersive X-ray spectroscopy (EDX), X-ray diffraction (XRD), X-ray photoelectron spectroscopy (XPS), cyclic voltammetry (CV), and fuel cell tests. Compared to the commercial Pd/XC-72 catalyst, the Pd-S-HCNFs show significantly higher electrocatalytic activity toward formic acid, methanol and ethanol in alkaline media, with a better stability.

2. Materials and methods

2.1. Chemicals

Palladium acetate (99.98%), benzyl mercaptan (99%), formic acid (98–100%) p.a. grade, and N,N-dimethylformamide were purchased from Sigma–Aldrich. Hydrazine hydrate (80% in water) and methanol (analytical grade) are from Merck Corporation in Germany. Nafion™ solution (5 wt% in water and light alcohols, Du Pont, DE520) was purchased from Ion Power, Inc. Ethanol and potassium hydroxide are supplied by Eka Chemicals AB and Solveco AB, respectively. Vulcan XC-72 carbon decorated with 20% Pd was purchased from Premetek Co. Ltd. All these chemicals are used as received without further purification. All aqueous solutions were prepared with distilled water.

2.2. Preparation of Pd-S-HCNFs

High quality HCNFs were synthesized according to our earlier report [32] using Pd_2C_{60} as catalyst in a standard CVD system [33]. 20 mg HCNFs were added into 20 mL ethanol containing 10 μL benzyl mercaptan and stirred overnight. The obtained thiol-functionalized HCNFs were separated by filtration and washed with ethanol and acetone three times to completely remove the excess benzyl mercaptan that did not attach onto the HCNF surface via π–π interaction. Thereafter the as-prepared material was dried for 2 h in an oven and labeled as S-HCNFs. 20 mg S-HCNFs were added into 10 mL ethanol and ultrasonicated for about 10 s and subsequently stirred. Then 20 μL of hydrazine solution were injected into the above-mentioned suspension and violently stirred at a speed of 700 rpm for 10 min followed by dropping 5 mL ethanol in which 11.2 mg $Pd(Ac)_2$ was dissolved into the solution while stirring for another 2 h to fully reduce the Pd ions. The suspension was centrifuged at a speed of 3000 rpm and carefully washed with ethanol and acetone for three rounds. After that, the as-obtained material was dried at 100 °C in an oven overnight and labeled as Pd-S-HCNFs. A schematic of the preparation is shown in Scheme 1.

2.3. Characterization of material

The structural analysis of the as-prepared materials was carried out on a transmission electron microscope (JEOL-JEM-2100) with an acceleration voltage of 200 kV. Holey carbon film-coated copper grids were used for the TEM study. X-ray diffraction of Pd-S-HCNFs was performed on a Siemens D5000 using Cu Kα (λ = 1.5406 Å) radiation. The accelerating voltage and the applied current were 40 kV and 30 mA, respectively. X-ray photoelectron spectroscopy was conducted on an AXIS Ultra DLD (Kratos Analytical Ltd., UK). Thermogravimetric analysis (TGA) was conducted in a Mettler Toledo TGA/DSC 1 LF/948 by heating to 900 °C in pure oxygen.

2.4. Electrocatalytic measurement

The electrocatalytic activity testing of the materials was performed on an Autolab PGSTAT30 with a three-electrode cell at room temperature (about 22 °C). A Pt wire and a saturated calomel electrode were used as counter and reference electrodes, respectively. A glassy carbon electrode coated with the catalyst was used as the working electrode. The working electrode was prepared as follows: (i) the glassy carbon electrode was carefully polished with 0.05 μm aluminum oxide paste on a chamois and then washed in acetone, ethanol and water under ultrasonication for 5 min, subsequently; (ii) 2 μL Pd/XC-72 (or Pd-S-HCNFs) suspension mixed with DMF (2 mg mL^{-1}) was dropped onto the electrode surface (0.07 cm^2) and dried in room temperature; (iii) 4 μL of Nafion™ solution (0.05 wt% in water and light alcohols, Ionpower Inc.) was deposited on the surface of the catalyst-modified glassy carbon electrode and dried in air without any heating process. 1 M KOH was used as the electrolyte solution during the electrochemical measurement. Prior to each measurement, the test solution was bubbled with argon for at least 30 min to remove dissolved oxygen.

For fuel cell tests, Pd/XC-72 (or Pd-S-HCNFs) was mixed by ultrasonication for 30 min with water and 5 wt% Nafion™ solution. The weight ratio was 1:15:3. The resulting ink was drop casted by a Pasteur pipette on a carbon-cloth diffusion layer (carbon cloth B-1, designation A, Clean Fuel Cell Energy). The cathode consisted

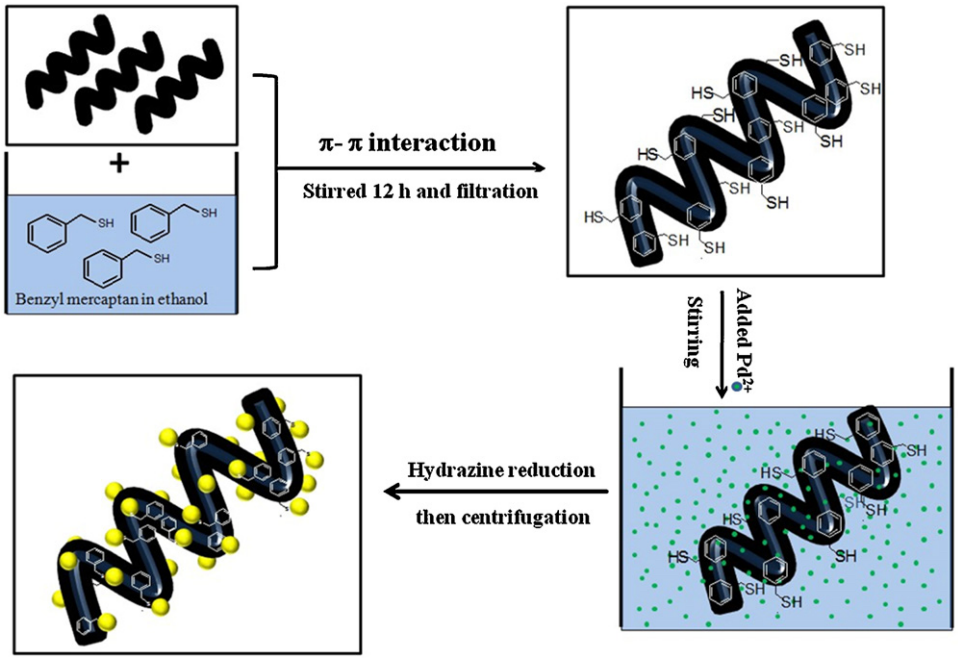

Scheme 1. Preparation procedure for Pd-S-HCNFs.

of standard 60 wt% Pt/Vulcan catalyst (BASF Fuel Cell) at a Pt loading of 4 mg/cm^{-2}. One side of the cathode-side carbon-cloth was Teflon^{TM}-coated for better water management. The cathode ink was painted on this side of carbon-cloth. Electrode assemblies were formed by hot pressing (0.8 kg cm^{-2}, 130 °C, 20 min) of Nafion^{TM} 115 membrane, with anode and cathode. The fuel cell tests were conducted at 30 °C and ambient pressure. The anode and cathode were fed 3 M aqueous formic acid solution at a flow rate of 0.5 mL min^{-1} and O_2 at a flow rate of 1.0 L min^{-1}, respectively. The output voltage as a function of applied current was measured.

3. Results and discussion

3.1. HR-TEM and TGA analysis

Fig. 1a shows a representative bright-field TEM image of the HCNFs with diameters about 60 nm. The HCNFs used in our study are similar to the material reported in our previous study which showed that more than 90% of the synthesized nanostructures have helical shape with uniform pitch and homogeneous diameters in the range of 40–60 nm [32]. The unique shape of the HCNFs makes them to potential candidates as catalyst support, in a similar way as some other carbon nanostructures such as coiled and bamboo-like carbon nanotubes [34–36]. Fig. 1b shows the general morphology of Pd decorated HCNFs (Pd-S-HCNF). The Pd nanoparticles are uniformly attached at the surface of HCNFs without any significant accumulation. This is the case, even after storage for three months in ethanol solution, which is significantly better than reported for non-covalent self-assembly methods [15], indicating that these nanoparticles are strongly fixed on the HCNF surface. A higher magnification of the selected area (Fig. 1c) shows that the Pd nanoparticles are crystalline and well-defined with diameter from 3 to 7 nm (average diameter 4.9 ± 1.2 nm, see supporting information for statistical size profiles). The crystallinity is confirmed also by selected area electron diffraction (SAED) (supporting information). In only very few spots we could observe that Pd nano crystals had accumulated into larger clusters. The commercial Pd/XC-72 catalyst was also characterized by TEM (supporting information, S3) which shows that the Pd-particles have diameters from 4 to 8 nm (average diameter 5.7 ± 1.4 nm). The external loading of the Pd/HCNFs and Pd/XC-72 was determined by TGA to 19% and 21.5%, respectively (Figs. S4 and S5).

3.2. Energy dispersive analysis of X-ray

The EDX spectrum (Fig. 1d) of the Pd-S-HCNFs confirms the presence of palladium, sulfur, and carbon in the sample and supports that the Pd nanoparticles are strongly fixed on the benzyl mercaptan functionalized HCNF surface via Pd—S covalent bonds. The atomic ratio of Pd to S on the functionalized materials is very high, supporting that the Pd nanoparticles are not covered with sulfur groups but only "use" the sulfur as anchor to the HCNFs. This is in agreement with XPS data that detects sulfur groups in the undecorated functionalized HCNFs but not in the Pd-S-HCNFs due to the screening of Pd nano particles on top of the sulfur groups (see supporting information). The Cu, Si and Cr peaks originate from the copper TEM grid, the synthesis process, and the TEM microscope, respectively.

3.3. XRD analysis of Pd-S-HCNFs

The inset in Fig. 1b shows the XRD spectrum of the Pd-S-HCNFs. Three peaks at $2\theta = 39.8°$, 46.4° and 68.1° are assigned to the (1 1 1), (2 0 0) and (2 2 0) crystalline planes of the face centered cubic structure of Pd. The lattice constant of the Pd nanoparticles derived from the (2 2 0) peak is 3.89 Å in good agreement with the electron diffraction data obtained in HR-TEM (supporting information). It has been reported that the lattice parameter can have a clear influence on the catalytic performance in a fuel cell [37]. From Scherrer's fomula [38,39], the crystallite size of Pd-S-HCNFs is estimated to about 5.1 nm, which is in excellent agreement with the TEM results.

3.4. Electrocatalytic performance of catalyst

To investigate the electrocatalytic performance of the as-produced Pd-S-HCNFs, a series of cyclic voltammetry (CV) measurements have been carried out in argon-saturated KOH solution. Fig. 2 shows the CV curves of the Pd-S-HCNFs and

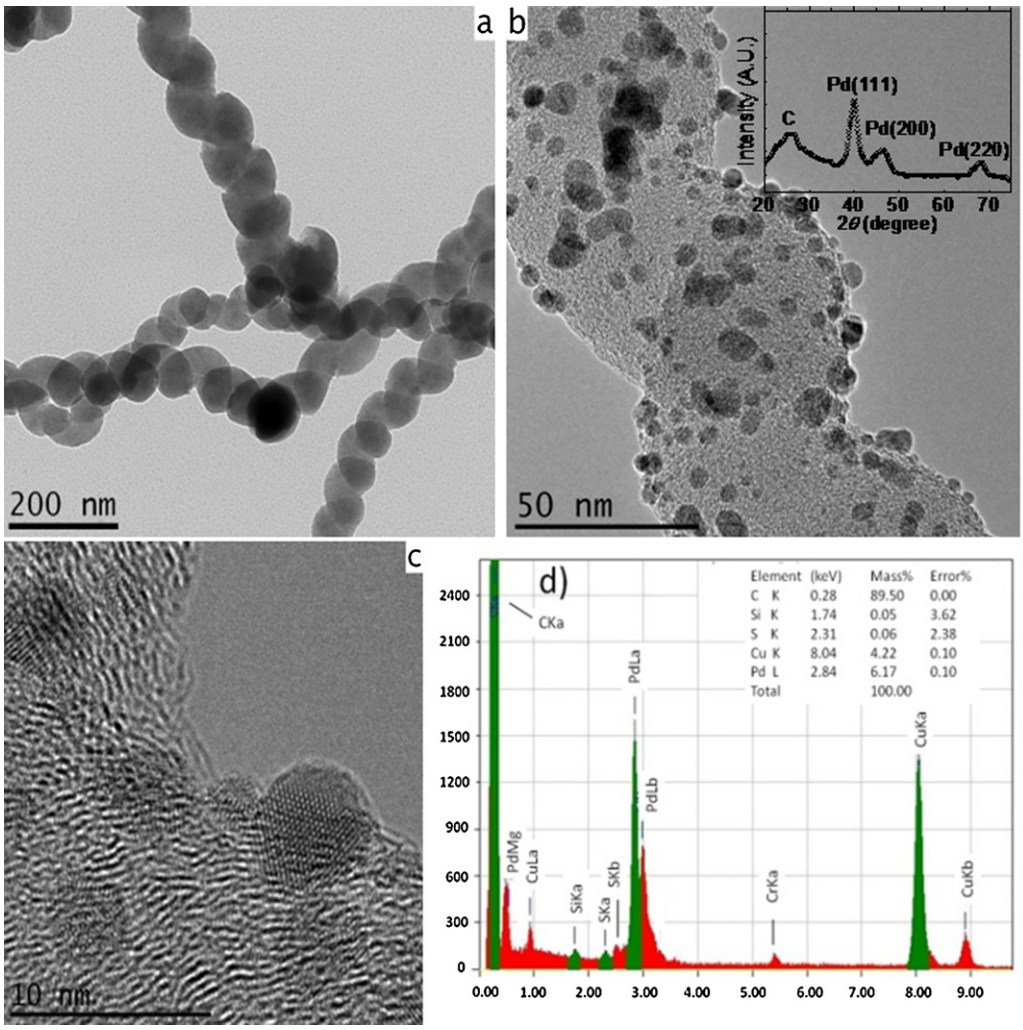

Fig. 1. TEM images of HCNFs (a) and Pd-S-HCNFs (b); (c) magnification of Pd-S-HCNFs, (d) energy dispersive X-ray spectrum of the sample displayed in (c). Inset in (b) shows the XRD pattern of the as-prepared Pd-S-HCNFs.

commercial Pd/XC-72 modified electrodes in blank solution without any fuel molecules. Both for the Pd-S-HCNF- and the Pd/XC-72 -modified electrodes, the oxidation peak around −0.5 V and the reduction peaks around −0.9 V can be assigned to redox peaks of oxygen-containing groups at the carbon support surface. The weak broad oxidation peak at the potential of −0.2–0.2 V corresponds to the electrochemical oxidation of Pd(0) on the electrode surface [40]. The reduction of Pd oxide occurs at the potential of −0.40 V for Pd-S-HCNFs and −0.43 V for Pd/XC-72, showing a decrease of 30 mV compared to that of the commercial catalyst. In addition, the peak shape of Pd oxide on the HCNFs is narrower than that of the commercial support XC-72, indicating a faster electron-transfer process between the HCNFs and the electrode surface. The fast electron transfer mechanism of Pd-decorated HCNFs is also manifested by a smaller separation of the primary anodic and cathodic redox peaks (E_{pa} = −0.55 V and E_{pc} = −0.89 V) of oxygen-containing groups on the HCNFs (0.34 V), than the corresponding value for XC-72 which is roughly 0.43 V (E_{pa} = −0.49 V and E_{pc} = −0.92 V). The reduction peak current of the Pd-S-HCNFs is 129 μA, which is almost identical to that of the Pd/XC-72 (132 μA) shows that the electroactive area of Pd-S-HCNFs is equal to that of the commercial catalyst.

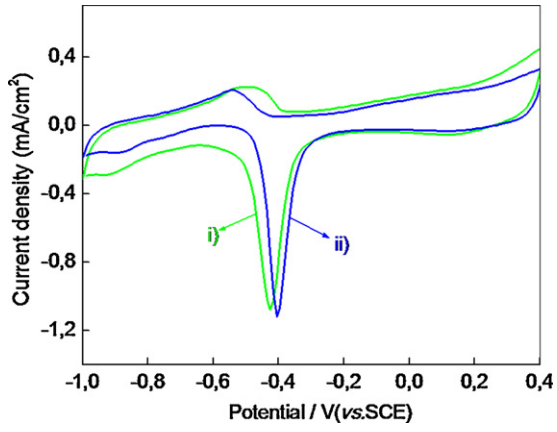

Fig. 2. CV curves of the Pd/XC-72 (i, green line) and Pd-S-HCNFs (ii) modified electrodes in argon-saturated 1 M KOH solution, scanning rate: 50 mV s^{-1}. (For interpretation of the references to color in this figure legend, the reader is referred to the web version of the article.)

3.5. Electrocatalytical oxidation of methanol and ethanol

Ethanol and methanol are important compounds in fuel cells, and are widely used in various industrial and technological fields. In fuel cells, ethanol possesses a series of advantages such as non-toxicity, high power density, renewability and zero pollution emission [3]. Pd-based nanomaterial shows special electrocatalytic activity toward ethanol in alkaline condition [41]. Carbon

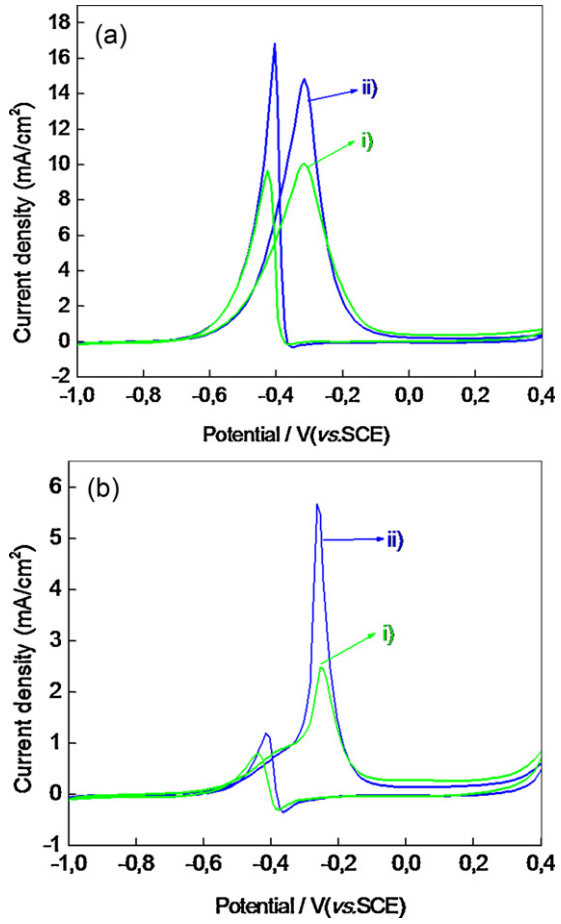

Fig. 3. (a) CV response of 0.5 M ethanol at the Pd/XC-72 (i, green line) and Pd-S-HCNFs (ii, blue line); (b) CV response of 0.5 M methanol at the Pd/XC-72 (i, green line) and Pd-S-HCNFs (ii, blue line) modified electrodes. Both measurements are performed in argon-saturated 1 M KOH solution at a scan rate of 50 mV s^{-1}. (For interpretation of the references to color in this figure legend, the reader is referred to the web version of the article.)

nanomaterials can also enhance the performance of Pd catalysts toward ethanol oxidation in alkaline media [42]. Direct methanol fuel cells are attractive due to their low temperature and pressure operation, quick refueling, good economy and simple cell design which makes it a promising candidate in fuel cell [43]. Pt based catalyst are easily poisoned to loss most of its catalysis activity toward methanol due to the strong adsorption of oxidation product CO at the Pt catalyst surface [44]. Pd based catalyst can avoid the formation of CO and shows good anti-poisoning ability toward CO and it is reported that Pd metal shows excellent activity for the electrocatalytic oxidation of methanol in alkaline media [45]. Fig. 3a and b shows the catalytic performance of Pd-S-HCNF and commercial Pd/XC-72 modified electrodes for ethanol and methanol oxidation, respectively. As seen in Fig. 3a, the onset potential of ethanol oxidation is at −0.65 V, which is similar to that of the commercial catalyst Pd/XC-72. The peak potential in forward scan is at about −0.32 V, whereas the peak potential of reverse scan is at −0.41 V, without a significant difference between the two different catalyst support. The oxidation mechanism of ethanol at the Pd-S-HCNFs in strong alkaline media is also described in a similar way by Zhao et al. [46], and Lin et al. [47].

$$Pd + CH_3CH_2OH \rightarrow Pd{-}(CH_3CH_2OH)_{ads} \quad (1)$$

$$Pd + HO^- \rightarrow Pd{-}OH_{ads} + e^- \quad (2)$$

$$Pd{-}(CH_3CH_2OH)_{ads} + 3HO^- \rightarrow Pd{-}(COCH_3)_{ads} + 3H_2O + 3e^- \quad (3)$$

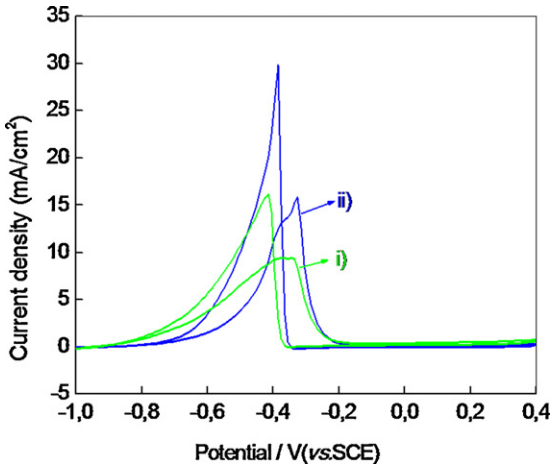

Fig. 4. CV curves response of 0.5 M formic acid at the Pd/XC-72 (i, green line) and Pd-S-HCNFs (ii, blue line) modified electrodes in argon-saturated 1 M KOH solution, scanning rate: 50 mV s^{-1}. (For interpretation of the references to color in this figure legend, the reader is referred to the web version of the article.)

$$Pd{-}(COCH_3)_{ads} + Pd{-}OH_{ads} \rightarrow 2Pd + CH_3COOH \quad \text{r.d.s.} \quad (4)$$

$$CH_3COOH + OH^- \rightarrow CH_3COO^- + H_2O \quad (5)$$

$$\text{Overall,} \quad CH_3CH_2OH + 5HO^- \rightarrow CH_3COO^- + 4H_2O + 4e^- \quad (6)$$

The oxidation peak current of ethanol at the as-produced Pd-S-HCNF is 1.5-fold higher than that of the Pd/XC-72, demonstrating that the as-produced materials is more efficient toward ethanol oxidation and can easily be reduced by ethanol to form Pd metal with high activity.

Fig. 3b shows the electrocatalytic performance of Pd-S-HCNF and commercial Pd/XC-72 modified electrodes toward the methanol oxidation in alkaline electrolyte. The generally accepted oxidation mechanism of methanol in alkaline media is similar to the case of ethanol [48].

$$CH_3OH + 5OH^- \rightarrow HCOO^- + 4H_2O + 4e^- \quad (7)$$

As shown in Fig. 3b two anodic peaks related to the oxidation of methanol are observed at the potential of $E'_a = -0.26$ V in forward scan and $E''_a = -0.44$ V in reverse scan for both the Pd-S-HCNF and the commercial Pd/XC-72 catalyst. The peak current intensities at the forward scan are 5.80 and 2.50 mA cm^{-2} for Pd-S-HCNF and Pd/XC-72, respectively manifesting an oxidation current intensity that is about 2.3 times higher for the Pd-S-HCNF than for the Pd/XC-72 at similar electroactive area.

3.6. Electrocatalytical oxidation of formic acid

The use of direct formic acid as fuel in polymer electrolyte membrane fuel cells have received a rising interest in recent years due to its low-toxicity, non-flammability and low penetration efficiency [16,49]. Fig. 4 presents CV curves of Pd/XC-72 (a) and Pd-S-HCNFs modified electrodes in 1 M KOH solution containing 0.5 M formic acid at the scan rate of 50 mV s^{-1}. Two clear oxidation peaks are observed. The oxidation peak at −0.35 V is assigned to the oxidation of electronegative $HCOO^-$ at the electrode surface in the forward scanning. The second oxidation peak at −0.38 V in the reverse scan is also the result of the residual carbon species formed in the forward scan. As the CV curves of formic acid at both the Pd-S-HCNFs and the Pd/XC-72 modified electrode are similar to these of ethanol in strong alkaline solution and quite different from these of formic acid in acidic or weak alkaline media [50], it is reasonable to suggest that oxidation of formic acid in strong alkaline media has a similar oxidation mechanism with that of ethanol using Pd catalyst. The

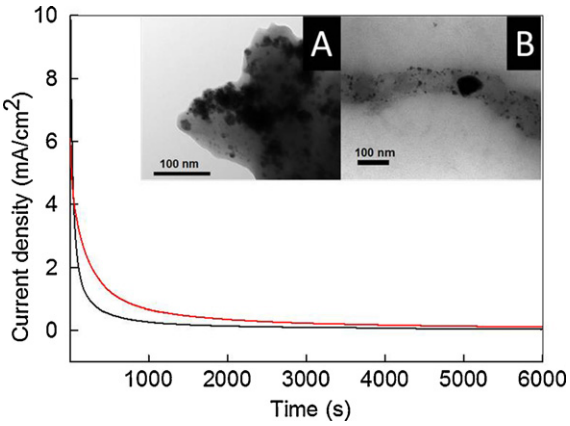

Fig. 5. Chronoamperometric curves of (i) Pd/XC-72- and (ii) Pd-S-HCNF-modified electrodes in 1 M KOH + 0.5 M HCOOH at −0.38 V. The inset shows TEM micrographs after 6000 s of chronoamperometric measurements for (A) of Pd/XC-72, and (B) Pd-S-HCNFs. The large Pd-particle in the middle of the HCNF is intrinsic and originates from the synthesis of the HCNFs [32].

oxidation mechanism of formic acid at the Pd-S-HCNFs in strong alkaline media can be described by;

$$HCOOH + OH^- \rightarrow HCOO^- + H_2O \quad (8)$$

$$Pd + HO^- \rightarrow Pd{-}OH_{ads} + e^- \quad (9)$$

$$2Pd + HCOO^- \rightarrow Pd{-}H_{ads} + Pd{-}(COO^-)_{ads} \quad (10)$$

$$Pd{-}(COO^-)_{ads} + 2HO^- \rightarrow CO_3{}^{2-} + Pd + H_2O + e^- \quad \text{r.d.s.} \quad (11)$$

$$Pd{-}OH_{ads} + Pd{-}H_{ads} \rightarrow 2Pd + H_2O \quad (12)$$

$$\text{Overall,} \quad HCOOH + 4HO^- \rightarrow CO_3{}^{2-} + 3H_2O + 2e^- \quad (13)$$

The onset potential of formic acid oxidation is −0.92 V on Pd/XC-72 and −0.74 V Pd-S-HCNF electrodes, respectively. The lower onset potential for ethanol oxidation on the Pd-S-HCNF modified electrode by 0.18 mV compared to the commercial catalyst Pd/XC-72 modified electrode indicates improved kinetics in the formic acid oxidation. This rationalizes that the peak current intensity is almost a factor 2 higher for the Pd-S-HCNFs (29.8 mA cm^{-2} at 0.386 V) compared to the Pd/XC-72 (15 mA cm^{-2} at 0.418 V).

3.7. Stability of Pd-S-HCNFs

The stability of the Pd-S-HCNFs was compared with the commercial catalyst Pd/XC-72 using chronoamperometric method. Fig. 5 presents the *i*–*t* curves of the Pd-S-HCNF- and Pd/XC-72-modified electrode in an argon saturated 1 M KOH solution containing 0.5 M formic acid, at a working potential of −0.3 V. Fig. 5 shows that the current density of formic acid oxidation at the Pd-S-HCNFs modified electrode is larger than that modified by Pd/XC-72 to times longer than 6000 s. Similar results were obtained for methanol and ethanol at the same experimental conditions. A possible explanation to the better stability of the catalytic activity of Pd-S-HCNFs can be attained by the TEM images (inset Fig. 5) showing the appearance of Pd/XC-72 and Pd-S-HCNFs after 6000 s of constant voltage of −0.38 V in chronoamperometric measurements. It is clear from the images that the Pd-particles on Pd/XC-72 are severely agglomerated while the Pd-particles on Pd-S-HCNFs show only small signs of agglomeration (the large particle in the middle of the HCNF is an intrinsic Pd-particle originating from the synthesis of the HCNFs). This supports the strong anchoring of the Pd-particles to the HCNFs by the linking of thiol groups as discussed for the XPS data.

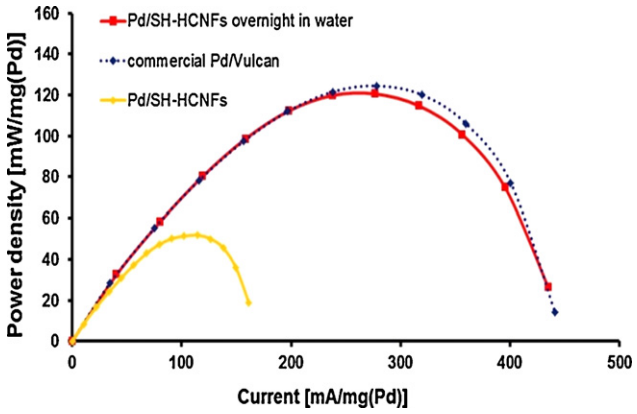

Fig. 6. Power density of Pd-S-HCNFs and Pd/XC-72 in a formic acid fuel cell.

3.8. Fuel cell tests

In a final test of the catalytic activity we have tested the Pd-S-HCNFs as anodic fuel cell catalyst as shown in Fig. 6. The power density for the as prepared material is relatively low but after one night of treatment in water the power density is high as for Pd/XC-72. The water activation treatment has been reported earlier for Pd-catalysts in fuel cells [51].

4. Conclusions

We have reported a novel self-assembly method to functionalize helical carbon nanofibers with Pd nanocrystals. TEM images of the as-prepared materials show that the nanofibers' surface was uniformly adhered with about 5 nm large Pd nanocrystals. The electrochemical response for formic acid, ethanol and methanol oxidation at the Pd-S-HCNFs modified electrode was investigated with CV and in fuel cell tests. Our results demonstrate that both stability and electrocatalytic activity of Pd-S-HCNFs is significantly better than that of commercial catalyst Pd/XC-72. We attribute this to the high crystallinity of the Pd nanoparticles, their uniform structure, the good conductivity of helical carbon nanofibers and the strong attachment of the nanocatalysts to the carbon support.

Our studies also show that helical carbon nanofibers are an excellent support of relative-cheap Pd nanocatalysts in direct fuel cells (DFCs). We have reasons to believe that further studies will reveal that the Pd-S-HCNFs also will find applications as high performance catalysts, effective sensors, and electric generation devices.

Acknowledgments

This work has been supported by Vetenskapsrådet (dnr-2010 3973), Ångpanneföreningen, Gustaf Richerts stiftelse. T. Wågberg thanks Magnus Bergvalls stiftelse and Kempestiftelsen for generous support. T. Wågberg and G.Z. Hu thanks Wenner-Gren stiftelsen for support. T. Sharifi thanks Kempestiftelsen for generous support. F. Nitze thanks Gustaf Richerts stiftelse. A. Borodzinski thanks the Polish Ministry of Science and Higher Education for financial support through the NCN project 2011/01/B/STS/03888. The Knut and Alice Wallenberg Foundations are acknowledged for an equipment grant for the electron microscopy facilities in Stockholm University.

Appendix A. Supplementary data

Supplementary data associated with this article can be found, in the online version, at doi:10.1016/j.jpowsour.2012.02.080.

References

[1] B.C.H. Steele, A. Heinzel, Nature 414 (2001) 345–352.
[2] J. Kaiser, P.A. Simonov, V.I. Zaikovskii, C. Hartnig, L. Jorissen, E.R. Savinova, J. Appl. Electrochem. 37 (2007) 1429–1437.
[3] S.Q. Song, P. Tsiakaras, Appl. Catal. B: Environ. 63 (2006) 187–193.
[4] D.R. Kauffman, Y.F. Tang, P.D. Kichambare, J.F. Jackovitz, A. Star, Energy Fuels 24 (2010) 1877–1881.
[5] E. Agel, J. Bouet, J.F. Fauvarque, J. Power Sources 101 (2001) 267–274.
[6] P.C. Su, C.C. Chao, J.H. Shim, R. Fasching, F.B. Prinz, Nano Lett. 8 (2008) 2289–2292.
[7] C. Wang, M. Waje, X. Wang, J.M. Tang, R.C. Haddon, Y.S. Yan, Nano Lett. 4 (2004) 345–348.
[8] S. Trogisch, J. Hoffmann, L.D. Bertrand, J. Power Sources 145 (2005) 632–638.
[9] C.S. Song, Catal. Today 77 (2002) 17–49.
[10] R. Dillon, S. Srinivasan, A.S. Arico, V. Antonucci, J. Power Sources 127 (2004) 112–126.
[11] P.K. Shen, C.W. Xu, Electrochem. Commun. 8 (2006) 184–188.
[12] W.P. Zhou, A. Lewera, R. Larsen, R.I. Masel, P.S. Bagus, A. Wieckowski, J. Phys. Chem. B 110 (2006) 13393–13398.
[13] W.J. Zhou, J.Y. Lee, J. Phys. Chem. C 112 (2008) 3789–3793.
[14] W.X. Niu, Z.Y. Li, L.H. Shi, X.Q. Liu, H.J. Li, S. Han, J. Chen, G.B. Xu, Cryst. Growth Des. 8 (2008) 4440–4444.
[15] W. Yang, X.L. Wang, F. Yang, C. Yang, X.R. Yang, Adv. Mater. 20 (2008) 2579.
[16] X.W. Yu, P.G. Pickup, J. Power Sources 182 (2008) 124–132.
[17] E. Antolini, Appl. Catal. B: Environ. 88 (2009) 1–24.
[18] Y. Zhu, Y.Y. Kang, Z.Q. Zou, Q. Zhou, J.W. Zheng, B.J. Xia, H. Yang, Electrochem. Commun. 10 (2008) 802–805.
[19] Z.P. Sun, X.G. Zhang, H. Tong, Y.Y. Liang, H.L. Li, J. Colloid Interface Sci. 337 (2009) 614–618.
[20] Z. Wang, Z.Z. Zhu, Y.X. Li, H.L. Li, Chin. J. Chem. 26 (2008) 666–670.
[21] G.W. Yang, G.Y. Gao, G.Y. Zhao, H.L. Li, Carbon 45 (2007) 3036–3041.
[22] O. Winjobi, Z. Zhang, C. Liang, W. Li, Electrochim. Acta 55 (2010) 4217–4221.
[23] S. Chakraborty, C.R. Raj, Carbon 48 (2010) 3242–3249.
[24] H. Zhao, J. Yang, L. Wang, C.G. Tian, B.J. Jiang, H.G. Fu, Chem. Commun. 47 (2011) 2014–2016.
[25] K. Hernadi, L. Thien-Nga, L. Forro, J. Phys. Chem. B 105 (2001) 12464–12468.
[26] H.S. Jung, S.Y. Lee, J.P. Ahn, J.K. Park, Met. Mater. Int. 12 (2006) 417–423.
[27] H. Raghubanshi, S.L. Hudson, O.N. Srivastava, Int. J. Hydrogen Energy, 2011.
[28] N.J. Tang, W. Zhong, A. Gedanken, Y.W. Du, J. Phys. Chem. B 110 (2006) 11772–11774.
[29] L.Y. Yu, L. Sui, Y. Qin, Z.L. Cui, Chem. Eng. J. 144 (2008) 514–517.
[30] T. Hyeon, S. Han, Y.E. Sung, K.W. Park, Y.W. Kim, Angew. Chem. Int. Ed. 42 (2003) 4352–4356.
[31] M. Sevilla, C. Sanchis, T. Valdes-Solis, E. Morallon, A.B. Fuertes, Electrochim. Acta 54 (2009) 2234–2238.
[32] F. Nitze, E. Abou-Hamad, T. Wågberg, Carbon 49 (2011) 1101–1107.
[33] F. Nitze, B.M. Andersson, T. Wågberg, Phys. Status Solidi (b) 246 (2009) 2440–2443.
[34] K.T. Lau, M. Lu, D. Hui, Compos. B: Eng. 37 (2006) 437–448.
[35] N. Tang, J. Wen, Y. Zhang, F. Liu, K. Lin, Y. Du, ACS Nano 4 (2010) 241–250.
[36] X.A. Xu, S.J. Jiang, Z. Hu, S.Q. Liu, ACS Nano 4 (2010) 4292–4298.
[37] Y.J. Huang, X.C. Zhou, J.H. Liao, C.P. Liu, T.H. Lu, W. Xing, Electrochem. Commun. 10 (2008) 1155–1157.
[38] A.L. Patterson, Phys. Rev. 56 (1939) 978–982.
[39] L. Xu, X.C. Wu, J.J. Zhu, Nanotechnology 19 (2008) 6.
[40] V.C. Diculescu, A.M. Chiorcea-Paquim, O. Corduneanu, A.M. Oliveira-Brett, J. Solid State Electrochem. 11 (2007) 887–898.
[41] H. Wang, C.W. Xu, F.L. Cheng, S.P. Jiang, Electrochem. Commun. 9 (2007) 1212–1216.
[42] H.T. Zheng, Y.L. Li, S.X. Chen, P.K. Shen, J. Power Sources 163 (2006) 371–375.
[43] T. Ito, K. Kimura, M. Kunimatsu, Electrochem. Commun. 8 (2006) 973–976.
[44] Q. Wang, G.Q. Sun, L.H. Jiang, Q. Xin, S.G. Sun, Y.X. Jiang, S.P. Chen, Z. Jusys, R.J. Behm, Phys. Chem. Chem. Phys. 9 (2007) 2686–2696.
[45] L.D. Burke, K.J. Odwyer, Electrochim. Acta 35 (1990) 1821–1827.
[46] Z.X. Liang, T.S. Zhao, J.B. Xu, L.D. Zhu, Electrochim. Acta 54 (2009) 2203–2208.
[47] S.C. Lin, J.Y. Chen, Y.F. Hsieh, P.W. Wu, Mater. Lett. 65 (2011) 215–218.
[48] R.K. Pandey, V. Lakshminarayanan, J. Phys. Chem. C 113 (2009) 21596–21603.
[49] S.X. Zhang, M. Qing, H. Zhang, Y.N. Tian, Electrochem. Commun. 11 (2009) 2249–2252.
[50] F. Nitze, M. Mazurkiewicz, A. Malolepszy, A. Mikolajczuk, P. Kedzierzawski, C.W. Tai, G.Z. Hu, J.K. Kurzydlowski, L. Stobinski, A. Borodzinski, T. Wågberg, Electrochim. Acta 63 (2012) 323–328.
[51] Y. Zhou, J. Liu, J. Ye, Z. Zou, J. Ye, J. Gu, T. Yu, A. Yang, Electrochim. Acta 55 (2010) 5024–5027.